Journal of Marine Science and Technology

Volume 26 | Issue 3 Article 11

SHAPE OPTIMIZATION OF RECTANGULAR MULTI-CHAMBER MUFFLERS AT HIGH-ORDER-MODES

Ying-Chun Chang
Department of Mechanical Engineering, Tatung University, Taiwan, R.O.C

Min-Chie Chiu
Department of Mechanical and Automation Engineering, Chung Chou University of Science and Technology, Taiwan, R.O.C., minchie.chiu@msa.hinet.net

Recommended Citation

Chang, Ying-Chun and Chiu, Min-Chie (2018) "SHAPE OPTIMIZATION OF RECTANGULAR MULTI-CHAMBER MUFFLERS AT HIGH-ORDER-MODES," *Journal of Marine Science and Technology*: Vol. 26: Iss. 3, Article 11.
DOI: DOI: 10.6119/JMST.201806_26(3).0011
Available at: https://jmstt.ntou.edu.tw/journal/vol26/iss3/11

SHAPE OPTIMIZATION OF RECTANGULAR MULTI-CHAMBER MUFFLERS AT HIGH-ORDER-MODES

Acknowledgements

The authors acknowledge the financial support of the National Science Council (MOST 104-2221-E-036-027, R.O.C.).

Journal of Marine Science and Technology, Vol. 26, No. 3, pp. 397-407 (2018)
DOI: 10.6119/JMST.2018.06_(3).0011

SHAPE OPTIMIZATION OF RECTANGULAR MULTI-CHAMBER MUFFLERS AT HIGH-ORDER-MODES

Ying-Chun Chang[1] and Min-Chie Chiu[2]

Key words: eigen function, genetic algorithm, higher order mode, optimization.

ABSTRACT

Muffler design as of late has been restricted to lower frequencies using the plane wave theory. This has led to an underestimation of acoustical performances at higher frequencies. To overcome the above shortcomings, an analysis of three-dimensional waves propagating for a simple muffler using the finite element method has been developed. However, there has been scant research on rectangular mufflers equipped with baffle plates that eliminate noise, nor has the space-constrained conditions of industrial muffler designs been properly addressed. Therefore, to improve the acoustical performance of a rectangular muffler within a constrained space, the shape optimization of rectangular mufflers using an eigen function, a four-pole system in conjunction with a Genetic Algorithm is proposed and assessed. Here, a numerical analysis of pure tone noise emitted from an induced fan using three kinds of rectangular mufflers hybridized with multiple chambers is introduced. Before the optimization process is carried out, an accuracy check of the mathematical models for two rectangular one-chamber/three-chamber mufflers with various allocations of inlets/outlets and partitioned bafflers is also performed. Simulated results reveal that the acoustical performance of a muffler with more geometric design parameter is found to be more efficient. And finally, the STL of the muffler will increase as the number of the rectangular chambers increases.

I. INTRODUCTION

The researches of mufflers have been widely addressed. Munjal (1975) developed the advanced four-pole transfer matrix using the fluid dynamic theory. Sullivan and Crocker (1978, 1979) presented coupled equations for the outer and inner tubes of a perforated muffler. Jayaraman and Yam (1981) developed an analytic solution for the coupled equations. However, all the solutions obtained were based on the plane wave theory which neglected the acoustical effect of a higher order wave. To overcome this weakness, Ih and Lee (1985, 1897) introduced the acoustical performance of an expansion muffler with a circular section. Later, Venkatesham et al. (2009) analyzed the acoustical performance of a rectangular expansion chamber with arbitrary location of inlet/outlet using Green's functions. Abom (1990) deduced a four-pole matrix for an extended muffler with a circular section. Munjal (1987) simplified the calculation process using a numerical analysis method. This method can be easily used in the expansion muffler with rectangular and circular sections; however, the ratio of the expansion area to the inlet/outlet area should be an integer value. Additionally, it is difficult to analyze a muffler using the analytic method if the angle between inlet and outlet is 90 degrees. Because more calculation time is needed, this type of muffler is often analyzed using the finite element method (Young and Crocker, 1975) or the two-dimensional boundary element method (Seybert and Cheng, 1987). Ih (1992) developed a numerical method to analyze the acoustical performance of the expansion muffler hybridized with a circular/rectangular section and an inlet/outlet duct. The inlet/outlet ducts may be parallel with/without the same height, or they may be perpendicular to each other. Considering the orthogonality of modes in each chamber, Selamet and Ji (1998) developed a mathematical mode of circular flow-reversing chambers. To find the appropriate design parameters within a space-constrained situation, Yeh et al. (2004) and Chang et al. (2005) assessed shape optimizations of multi-segment and double-chamber mufflers using the plane wave theory. Yeh et al. (2006) analyzed and optimized a space-constrained reactive muffler in low frequencies in 2006. Similarly, Chiu and Chang (2008), developed multi-chamber perforated mufflers and explored the optimal muffler shapes under plane wave situation. Later, Chiu (2010a; 2010b; 2010c), proposed three kinds of mufflers (multi-chamber mufflers equipped with plug-inlet tube, one-chamber muffler equipped with reverse-flow ducts, and three-chamber mufflers hybridized with a side inlet and a perforated tube) and evaluated the best shape of the muffler. And, Chang et al. (2010) developed opti-

Paper submitted 05/09/17; revised 03/20/18; accepted 05/16/18. Author for correspondence: Min-Chie Chiu (e-mail: minchie.chiu@msa.hinet.net).
[1] Department of Mechanical Engineering, Tatung University, Taiwan, R.O.C.
[2] Department of Mechanical and Automation Engineering, Chung Chou University of Science and Technology, Taiwan, R.O.C.

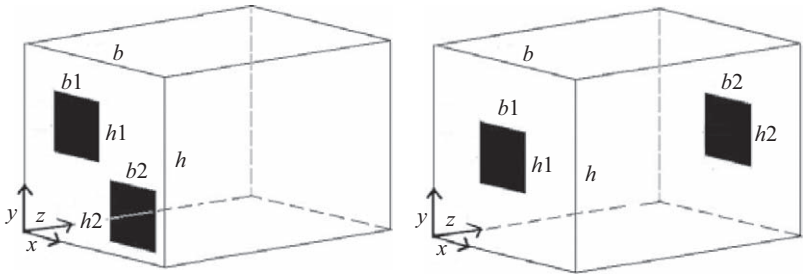

(a) A rectangular reverse muffler (b) A rectangular straight muffler

Fig. 1. Mechanism of a rectangular one-chamber muffler.

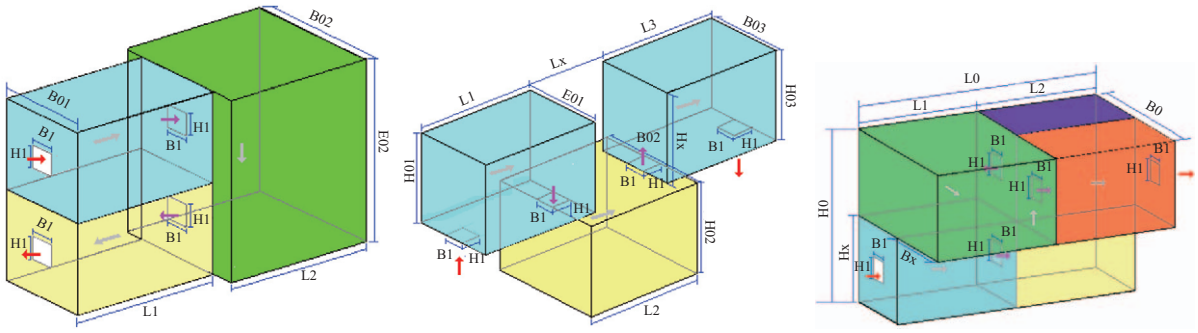

(a) muffler A: a stacked three-chamber muffler (b) muffler B: a parallel three-chamber muffler (c) muffler C: a stacked four-chamber muffler

Fig. 2. Mechanisms for three kinds of rectangular multi-chamber mufflers (muffler A: a stacked three-chamber muffler; muffler B: a parallel three-chamber muffler; muffler C: a stacked four-chamber muffler).

mally shaped one-chamber mufflers equipped with perforated intruding tubes using a SA Method. Later, Chiu and Chang (2011a, 2011b, 2013) presented three kinds of optimally shaped mufflers (two-chamber mufflers with perforated plug/non-plug tubes, multi-chamber perforated mufflers, and multi-chamber side inlet/outlet mufflers hybridized with multiple perforated intruding tubes). Subsequently, Chiu (2013) presented one-chamber perforated mufflers filled with wool and explored its optimal shape. However, the effect of higher order wave was ignored. So, considering the high-order-mode wave effect, Chiu and Chang (2014) investigated the acoustical performance of mufflers which has one-chamber and inlet and outlet. Mimani and Munjal (2016a, 2016b), developed an optimal design on reactive rectangular expansion chambers and flow-reversal end-chamber mufflers. Because of simple shape and few chamber (one chamber) design for the muffler, the noise abatement in eliminating high noise is insufficient; therefore, in order to enhance the acoustical performance, three kinds of complicated mufflers hybridized with multiple rectangular chambers (muffler A: a stacked three-chamber muffler; muffler B: a parallel three-chamber muffler; muffler C: a stacked four-chamber muffler) in conjunction with a GA method are proposed.

II. THEORETICAL BACKGROUND

Concerning the higher order wave, the mathematical models of two rectangular one-chamber mufflers with different allocations of inlets and outlets shown in Fig. 1 will be deduced. In order to enhance the acoustical performance of the muffler, three kinds of rectangular mufflers (muffler A: a stacked three-chamber muffler; muffler B: a parallel three-chamber muffler; muffler C: a stacked four-chamber muffler) with multiple chambers shown in Fig. 2 are proposed. Based on the analysis of the higher order modes, the acoustical performances of rectangular mufflers A-C will be established. Finally, the objective functions of the three mufflers at a target tone will be constructed.

1. Derivation of Mathematical Models

The sound wave for one-chamber rectangular mufflers is shown in Fig. 1. As derived by Ih (1992) and Venkatesham et al. (2009), when the inlet and outlet are on the same side or opposite side, the acoustical pressure at inlet ($\bar{p}_{11}$) and outlet ($\bar{p}_{22}$) are expressed as

$$\bar{p}_{11} = (-1)^1 jU_1 Z_0 \left\{ \frac{1}{\tan kl} + \left(\frac{bh}{b_1 h_1} \right)^2 \left[\sum \frac{1}{v_{m0}} \left(\frac{2}{m\pi} \right)^2 \left(\frac{h_1}{h} \right)^2 \psi_{111}^2 + \sum \frac{1}{v_{0n}} \left(\frac{2}{n\pi} \right)^2 \left(\frac{b_1}{b} \right)^2 \psi_{112}^2 + \sum\sum \frac{1}{v_{mn}} \left(\frac{4}{mn\pi^2} \right)^2 \psi_{111}^2 \psi_{112}^2 \right] \frac{k}{k_z \tan k_z l} \right\}$$

$$= (-1)^1 jU_1 Z_0 E_{11} \tag{1a}$$

$$\bar{p}_{22}=(-1)^2\,jU_2Z_0\left\{\frac{1}{\tan kl}+\left(\frac{bh}{b_2h_2}\right)^2\left[\sum\frac{1}{v_{m0}}\left(\frac{2}{m\pi}\right)^2\left(\frac{h_2}{h}\right)^2\psi_{221}^2+\sum\frac{1}{v_{0n}}\left(\frac{2}{n\pi}\right)^2\left(\frac{b_2}{b}\right)^2\psi_{222}^2+\sum\sum\frac{1}{v_{mn}}\left(\frac{4}{mn\pi^2}\right)^2\psi_{221}^2\psi_{222}^2\right]\frac{k}{k_z\tan k_zl}\right\}=(-1)^2\,jU_2Z_0E_{22} \tag{1b}$$

When the inlet and outlet are on the same side (Fig. 1(a)), the interactive average acoustical pressures ($\bar{p}_{12}$ and $\bar{p}_{21}$) derived by Ih (1992) and Venkatesham et al. (2009) are

$$\bar{p}_{12}=(-1)^2\,jU_2Z_0\left\{\frac{1}{\tan kl}+\left(\frac{bh}{b_1h_1}\right)\left(\frac{bh}{b_2h_2}\right)\left[\sum\frac{1}{v_{m0}}\left(\frac{2}{m\pi}\right)^2\left(\frac{h_1}{h}\right)\left(\frac{h_2}{h}\right)\psi_{121}\psi_{121}'+\sum\frac{1}{v_{0n}}\left(\frac{2}{n\pi}\right)^2\left(\frac{b_1}{b}\right)\left(\frac{b_2}{b}\right)\psi_{122}\psi_{122}'+\sum\sum\frac{1}{v_{mn}}\left(\frac{4}{mn\pi^2}\right)^2\psi_{121}\psi_{121}'\psi_{122}\psi_{122}'\right]\frac{k}{k_z\tan k_zl}\right\}=(-1)^2\,jU_2Z_0E_{12} \tag{2a}$$

$$\bar{p}_{21}=(-1)^1\,jU_1Z_0\left\{\frac{1}{\tan kl}+\left(\frac{bh}{b_2h_2}\right)\left(\frac{bh}{b_1h_1}\right)\left[\sum\frac{1}{v_{m0}}\left(\frac{2}{m\pi}\right)^2\left(\frac{h_2}{h}\right)\left(\frac{h_1}{h}\right)\psi_{211}\psi_{211}'+\sum\frac{1}{v_{0n}}\left(\frac{2}{n\pi}\right)^2\left(\frac{b_2}{b}\right)\left(\frac{b_1}{b}\right)\psi_{212}\psi_{212}'+\sum\sum\frac{1}{v_{mn}}\left(\frac{4}{mn\pi^2}\right)^2\psi_{211}\psi_{211}'\psi_{212}\psi_{212}'\right]\frac{k}{k_z\tan k_zl}\right\}=(-1)^1\,jU_1Z_0E_{21} \tag{2b}$$

Also, when the inlet and outlet are on the opposite side (Fig. 1(a)), the interactive average acoustical pressures ($\bar{p}_{12}$ and $\bar{p}_{21}$) are (Ih, 2009; Venkatesham et al., 2009)

$$\bar{p}_{12}=(-1)^2\,jU_2Z_0\left\{\frac{1}{\sin kl}+\left(\frac{bh}{b_1h_1}\right)\left(\frac{bh}{b_2h_2}\right)\left[\sum\frac{1}{v_{m0}}\left(\frac{2}{m\pi}\right)^2\left(\frac{h_1}{h}\right)\left(\frac{h_2}{h}\right)\psi_{121}\psi_{121}'+\sum\frac{1}{v_{0n}}\left(\frac{2}{n\pi}\right)^2\left(\frac{b_1}{b}\right)\left(\frac{b_2}{b}\right)\psi_{122}\psi_{122}'+\sum\sum\frac{1}{v_{mn}}\left(\frac{4}{mn\pi^2}\right)^2\psi_{121}\psi_{121}'\psi_{122}\psi_{122}'\right]\frac{k}{k_z\sin k_zl}\right\}=(-1)^2\,jU_2Z_0E_{12} \tag{3a}$$

$$\bar{p}_{21}=(-1)^1\,jU_1Z_0\left\{\frac{1}{\sin kl}+\left(\frac{bh}{b_2h_2}\right)\left(\frac{bh}{b_1h_1}\right)\left[\sum\frac{1}{v_{m0}}\left(\frac{2}{m\pi}\right)^2\left(\frac{h_2}{h}\right)\left(\frac{h_1}{h}\right)\psi_{211}\psi_{211}'+\sum\frac{1}{v_{0n}}\left(\frac{2}{n\pi}\right)^2\left(\frac{b_2}{b}\right)\left(\frac{b_1}{b}\right)\psi_{212}\psi_{212}'+\sum\sum\frac{1}{v_{mn}}\left(\frac{4}{mn\pi^2}\right)^2\psi_{211}\psi_{211}'\psi_{212}\psi_{212}'\right]\frac{k}{k_z\sin k_zl}\right\}=(-1)^1\,jU_1Z_0E_{21} \tag{3b}$$

For a one-chamber rectangular muffler having the inlet and outlet on the same side (Fig. 1(a)), using the superposition method at inlet and outlet and rearranging P and U, the acoustical transfer matrix between nodes 1 and 2 is

$$\begin{bmatrix}P_1\\U_1\end{bmatrix}=\begin{bmatrix}TS_{1,1}&TS_{1,2}\\TS_{2,1}&TS_{2,2}\end{bmatrix}\begin{bmatrix}P_2\\U_2\end{bmatrix} \tag{4a}$$

where

$$\begin{aligned}TS_{1,1}&=\left(\bar{P}_1/\bar{P}_2\right)|_{U_2=0}=E_{11}/E_{12},\\TS_{1,2}&=\left(\bar{P}_1/U_2\right)|_{\bar{P}_2=0}=jZ_0\left(E_{12}-E_{11}E_{22}/E_{12}\right),\\TS_{2,1}&=\left(U_1/\bar{P}_2\right)|_{U_2=0}=j\left(Z_0E_{12}\right)^{-1},\\TS_{2,2}&=\left(U_1/U_2\right)|_{\bar{P}_2=0}=E_{22}/E_{12}\end{aligned} \tag{4b}$$

Similarly, a one-chamber rectangular muffler having the inlet and outlet on the opposite side (Fig. 1(b)), the acoustical transfer matrix between nodes 1 and 2 is

$$\begin{bmatrix}P_1\\U_1\end{bmatrix}=\begin{bmatrix}TR_{1,1}&TR_{1,2}\\TR_{2,1}&TR_{2,2}\end{bmatrix}\begin{bmatrix}P_2\\U_2\end{bmatrix} \tag{5}$$

Based on the above derivation, the acoustical performances of mufflers A-C shown in Fig. 2 will be established as follows:

For muffler A, the system's four-pole matrix and STL are

$$\begin{bmatrix}P_1\\U_1\end{bmatrix}=\begin{bmatrix}TS1_{1,1}&TS1_{1,2}\\TS1_{2,1}&TS1_{2,2}\end{bmatrix}\begin{bmatrix}TR1_{1,1}&TR1_{1,2}\\TR1_{2,1}&TR1_{2,2}\end{bmatrix}\begin{bmatrix}TS2_{2,1}&TS2_{1,2}\\TS2_{2,1}&TS2_{2,2}\end{bmatrix}\begin{bmatrix}P_4\\U_4\end{bmatrix}=\begin{bmatrix}T_{T11}&T_{T12}\\T_{T21}&T_{T22}\end{bmatrix} \tag{6a}$$

$$STL_1(f,\ \bar{X}_4)=20\log\left[\frac{\left|T_{T11}+\frac{T_{T12}}{Z_2}+T_{T21}Z_1+T_{T22}(S_4/S_1)\right|}{2}\right] \tag{6b}$$

where

$$\bar{X}_1=\left(L_1,\,L_2,\,B_{01},\,B_{02},\,H_{02}\right) \tag{6c}$$

Similarly, for muffler B, the system's four-pole matrix and STL are

$$\begin{bmatrix}P_1\\U_1\end{bmatrix}=\prod_{m=1}^{3}\left[T_m(f)\right]\begin{bmatrix}P_4\\U_4\end{bmatrix}=\begin{bmatrix}T_{T11}&T_{T12}\\T_{T21}&T_{T22}\end{bmatrix}\begin{bmatrix}P_4\\U_4\end{bmatrix} \tag{7a}$$

$$STL_2(f, \bar{X}_2) = 20\log\left[\frac{\left|T_{T11} + \frac{T_{T12}}{Z_2} + T_{T21}Z_1 + T_{T22}(S_5/S_1)\right|}{2}\right] \quad (7b)$$

where m is the number of the chambers,

$$\begin{aligned} &\bar{X}_2 = \left(B_{01}, B_{02}, H_{02}\right), B_{01} = B_{03}, \\ &H_{01} = H_{03} = H_X, \\ &L_1 = L_2 = L_3 \end{aligned} \quad (7c)$$

Likewise, for muffler C, the system's four-pole matrix and STL are

$$\begin{bmatrix} P_1 \\ U_1 \end{bmatrix} = \prod_{m=1}^{4}\left[T_m(f)\right]\begin{bmatrix} P_5 \\ U_5 \end{bmatrix} = \begin{bmatrix} T_{T11} & T_{T12} \\ T_{T21} & T_{T22} \end{bmatrix}\begin{bmatrix} P_5 \\ U_5 \end{bmatrix} \quad (8a)$$

$$STL_3(f, \bar{X}_3) = 20\log\left[\frac{\left|T_{T11} + \frac{T_{T12}}{Z_2} + T_{T21}Z_1 + T_{T22}(S_6/S_1)\right|}{2}\right] \quad (8b)$$

where m is the number of the chambers,

$$\bar{X}_3 = \left(L_0, B_0, H_0\right), L_1 = L_2 \quad (8c)$$

2. Objective Function

By using the formulas of Eqs. (6)-(8), the objective functions used in the GA optimization with respect to each type of plenum are established. For muffler A, the objective function in maximizing the *STL* at one tone (f_1) is

$$OBJ_1 = STL_1(f_1, \bar{X}_1) \quad (9)$$

Similarly, for muffler B, the objective function in maximizing the *STL* at one tone (f_1) is

$$OBJ_2 = STL_2(f_1, \bar{X}_2) \quad (10)$$

Also, for muffler C, the objective function in maximizing the *STL* at one tone (f_1) is

$$OBJ_3 = STL_3(f_1, \bar{X}_3) \quad (11)$$

III. MODEL CHECK

Before performing the *GA* optimal simulation on rectangular mufflers, an accuracy check of the mathematical models on the mufflers (a one-chamber concentric reverse muffler and a three-chamber concentric straight muffler) is performed using the analytic solution from Ih (2009). As depicted in Figs. 3 and 4, the theoretical prediction from Eqs. (1)-(5) and Ih's analytic data are in agreement. Therefore, the proposed fundamental mathematical models for the multi-chamber rectangular mufflers with inlets and outlets on the same side or opposite side are acceptable. Consequently, the models linked with the numerical method are applied to the shape optimization of rectangular mufflers A-C shown in Fig. 2 in the following section.

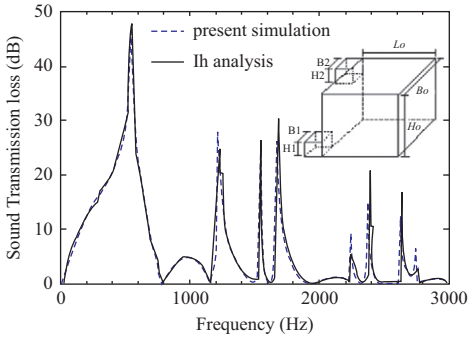

Fig. 3. Comparison of the simulated results of a rectangular one-chamber reverse muffler with Ih's analytic solution (muffler E: Bo = Ho = 0.15 m, B1 = B2 = H1 = H2 = 0.05 m, Lo = 0.025 m) (Ih, 1992).

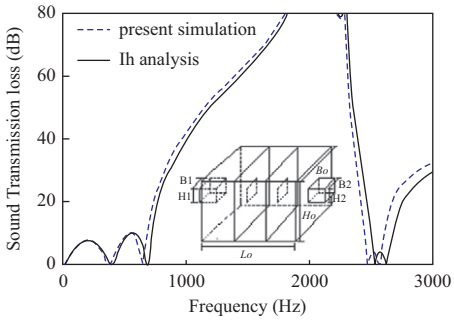

Fig. 4. Comparison of the simulated results of a rectangular three-chamber muffler with Ih's analytic solution (muffler F: Bo = Ho = 0.15 m, B1 = B2 = H1 = H2 = 0.05 m, Lo = 0.025 m) (Ih, 1992).

Obtaining the best acoustical performance by adjusting the design parameters, numerical assessments linked to a *GA* optimizer are applied. The corresponding *OBJ* functions and ranges of the design parameters are summarized in Eqs. (9)-(11) and Table 1.

IV. CASE STUDY

In this paper, an induced fan installed inside a machine room is used to convey the air from the machine to the atmosphere via a building's venting duct. In order to depress noise energy (I.D. fan) from the I.D. fan's outlet, three kinds of multi-chamber mufflers (mufflers A-C shown in Fig. 2) installed within a constrained space is proposed. Considering current geometric status, muffler A is designed as a stacked three-chamber muffler, muffler B is designed as a parallel three-chamber muffler, and muffler C

Table 1. Constrained conditions in the mufflers.

muffler A		
Design Parameters	Min. (m)	Max. (m)
L01	0.20	0.40
B01	0.10	0.30
L02	0.20	0.40
B02	0.10	0.30
H02	0.20	0.60
muffler B		
Design Parameters	Min. (m)	Max. (m)
B1	0.10	0.30
B2	0.10	0.30
H2	0.10	0.30
muffler C		
Design Parameters	Min. (m)	Max. (m)
L0	0.40	0.80
B0	0.30	0.50
H0	0.30	0.50

is planned as a stacked four-chamber muffler. Here, muffler B is attached onto the beam with a width of Lx and a height of Hx. Muffler C is attached onto the beam with a width of Bx and a height of Hx. The original sound power level (SWLO) has been investigated to be remarkable at 500 Hz. Here, the pure tone of 500 Hz is the fan's blade passing frequency (B_f) which has been obtained with $B_f = N_b$*rpm/60. Where N_b is the number of fan's blade and rpm is the revolution(s) per minute for the driven motor.

V. GENETIC ALGORITHM

Traditional gradient methods (such as EPFM, IPFM and FDM) need a good starting point before the optimization process is performed. However, the genetic algorithm (*GA*) does not need an appropriate starting point. Therefore, GA becomes easier to use. In addition, the GA's accuracy can be improved when all the GA parameters of crossover, mutation and elitism are taken into consideration (Chang et al., 2005). Here, the *GA* method used to search for the global optimum by imitating a genetic evolutionary process was formalized by Holland (1975) and extended to functional optimization by Jong (1975). It has been widely used in various fields (Yeh et al., 2004; Chang et al., 2005; Yeh et al., 2006; Chiu and Chang, 2008; Chiu, 2010; Chiu and Chang, 2014). For the GA optimization, design parameters of (X_1, X_2, …, X_k) were determined by searching for a better objective function (*OBJ*). Presetting the bit (the bit length of the chromosome) and the pop (the population number), the interval of the *k*-th design parameter (X_k) with $[Lb, Ub]_k$ was then mapped to the band of the binary value. The mapping system between the variable interval of $[Lb, Ub]_k$ and the k^{th} binary chromosome of

$$\underbrace{0\ 0\ 0\ 0\ \bullet\ \bullet\ \bullet\ 0\ 0\ 0}_{bit} \sim \underbrace{1\ 1\ 1\ 1\ \bullet\ \bullet\ \bullet\ 1\ 1\ 1}_{bit}$$

was then established. The encoding from *x* to *B*2*D* (binary to decimal) can be performed as

$$B2D_k = \text{integer}\left\{\frac{x_k - Lb_k}{Ub_k - Lb_k}(2^{bit} - 1)\right\} \tag{12}$$

By evaluating the *OBJ*, the whole set of chromosomes [$B2D_1$, $B2D_2$, …, $B2D_k$] that changed from binary form to decimal form was then assigned a fitness by decoding the transformation system.

$$\text{fitness} = OBJ(X_1, X_2, \ldots, X_k); \tag{13}$$

where

$$X_k = B2D_k * (Ub_k - Lb_k)/(2^{bit} - 1) + Lb_k$$

The GA operation is shown in Fig. 5. In order to assess an elitism of a gene, the tournament selection, a random comparison of the relative fitness from pairs of chromosomes, was adopted. In addition, one pair of offspring was generated from the selected parent via uniform crossover with a probability of *pc*. A mutation occurred with a probability of *pm* where the new and unexpected point was brought into the *GA* optimizer's search domain.

As indicated in Fig. 6, the process was terminated when the number of generations reached a pre-selected value of $iter_{\max}$.

VI. RESULTS AND DISCUSSION

1. Results

The accuracy of the *GA* optimization depends on five types of *GA* parameters including *pop* (population number), *bit*

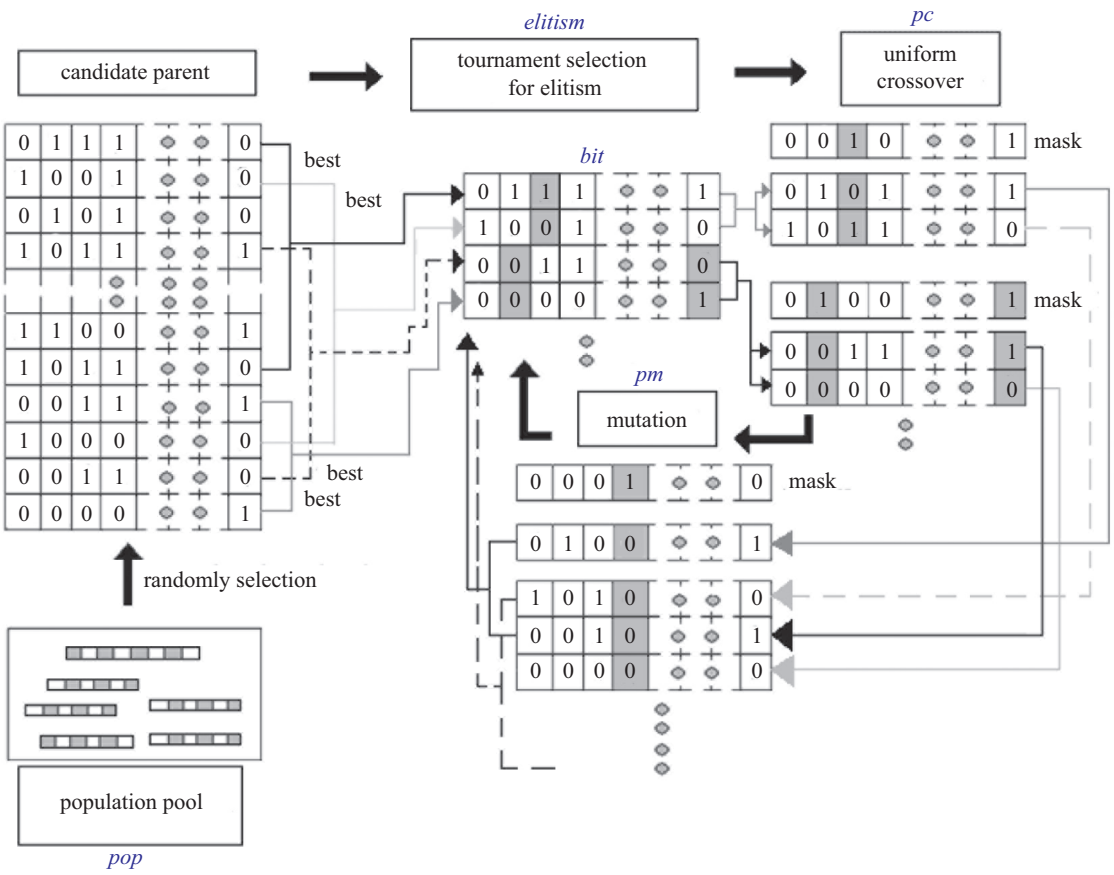

Fig. 5. Operations of the *GA* method.

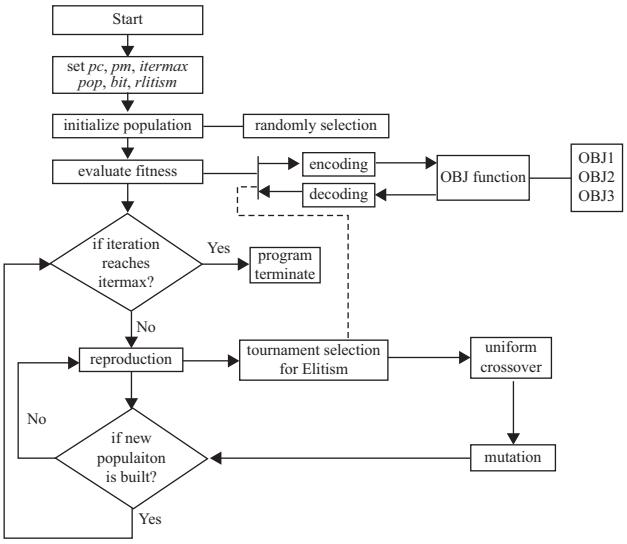

Fig. 6. Flow diagram of the *GA* method.

(chromosome length), *pc* (crossover rate), *pm* (mutation factor), and $iter_{max}$ (maximum iteration). To achieve a good optimization, the following parameters are varied step by step. The related GA control parameters used in the optimization are shown in Table 2.

Table 2. Selected GA parameters during shape optimization.

GA parameters	Value (or condition)
bit	20
pop	50
elitism	(tournament)
crossover	(uniform crossover)
pc	0.5
pm	0.5
$iter_{max}$	1000

Utilizing Eqs. (9)-(11) and using the *GA* parameters in the optimization process, the maximization of the $STL_1 \sim STL_3$ with respect to mufflers A-C at targeted tones (500 Hz, 1000 Hz, 2000 Hz) was performed and shown in Tables 3-5. As illustrated in Table 3, the STL of mufflers A-C at 500 Hz has been improved from 34 dB, 36 dB, 45 dB to 110 dB, 47 dB, and 125 dB. As can be seen in Table 4, the STL of mufflers A-C at 1000 Hz has been improved from 68 dB, 25 dB, and 100 dB to 115 dB, 70 dB, and 194 dB. Similarly, as depicted in Table 5, the STL of mufflers A-C at 2000 Hz has been improved from 30 dB, 27 dB, and 56 dB to 85 dB, 43 dB, and 140 dB.

Using this optimal design in a theoretical calculation, the com-

Table 3. Comparison of STL and design parameters of muffler A before and after the optimization (target tone of 500 Hz).

Target tone		Design Parameters					*OBJ*
		L1 (m)	B01 (m)	L2 (m)	B02 (m)	H02 (m)	STL - dB
Muffler A	original	0.30	0.20	0.30	0.20	0.40	34
	optimization	0.2032	0.2299	0.2360	0.2752	0.2150	110
Target tone		Design Parameters					*OBJ*
		B01 (m)		B02 (m)		H02 (m)	STL - dB
Muffler B	original	0.20		0.20		0.20	36
	optimization	0.3000		0.2391		0.2308	47
Target tone		Design Parameters					*OBJ*
		L0 (m)		B0 (m)		H0 (m)	STL - dB
Muffler C	original	0.60		0.40		0.40	45
	optimization	0.5586		0.3003		0.4719	125

Table 4. Comparison of STL and design parameters of muffler A before and after the optimization (target tone of 1000 Hz).

Target tone		Design Parameters					*OBJ*
		L1 (m)	B01 (m)	L2 (m)	B02 (m)	H02 (m)	STL - dB
Muffler A	original	0.30	0.20	0.30	0.20	0.40	68
	optimization	0.3250	0.2782	0.3028	0.1749	0.5735	115
Target tone		Design Parameters					*OBJ*
		B01 (m)		B02 (m)		H02 (m)	STL - dB
Muffler B	original	0.20		0.20		0.20	25
	optimization	0.2101		0.1614		0.1347	70
Target tone		Design Parameters					*OBJ*
		L0 (m)		B0 (m)		H0 (m)	STL - dB
Muffler C	original	0.60		0.40		0.40	100
	optimization	0.4757		0.4580		0.4633	194

Table 5. Comparison of STL and design parameters of muffler A before and after the optimization (target tone of 2000 Hz).

Target tone		Design Parameters					*OBJ*
		L1 (m)	B01(m)	L2 (m)	B02 (m)	H02 (m)	STL - dB
Muffler A	original	0.30	0.20	0.30	0.20	0.40	30
	optimization	0.3734	0.1688	0.2085	0.1658	0.3305	85
Target tone		Design Parameters					*OBJ*
		B01 (m)		B02 (m)		H02 (m)	STL - dB
Muffler B	original	0.20		0.20		0.20	27
	optimization	0.1739		0.2071		0.1726	43
Target tone		Design Parameters					*OBJ*
		L0 (m)		B0 (m)		H0 (m)	STL - dB
Muffler C	original	0.60		0.40		0.40	56
	optimization	0.4841		0.3608		0.4215	140

parison of *STL* curves with respect to mufflers A-C before and after optimization at targeted tones (500 Hz, 1000 Hz, 2000 Hz) are plotted in Figs. 7-9, Figs. 10-12, and Fig. 13-15. Consequently, the optimal *STL* curves with respect to mufflers A-C at targeted tone (500 Hz) is plotted in Fig. 16.

2. Discussion

As can be seen in Figs. 7-9, Figs. 10-12, and Fig. 13-15, the

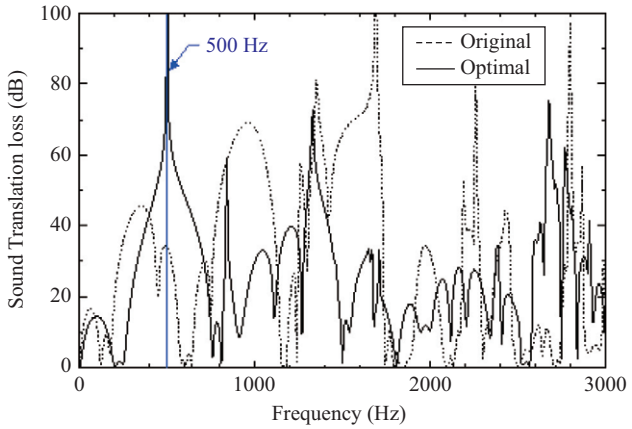

Fig. 7. Comparison of the STL of muffler A before and after optimization is performed (target tone: 500 Hz).

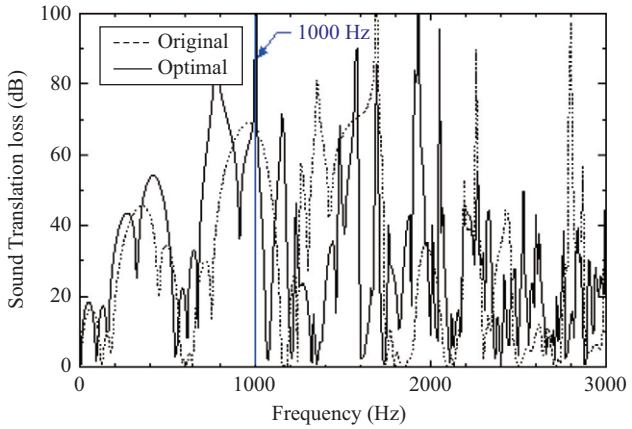

Fig. 10. Comparison of the STL of muffler A before and after optimization is performed (target tone: 1000 Hz).

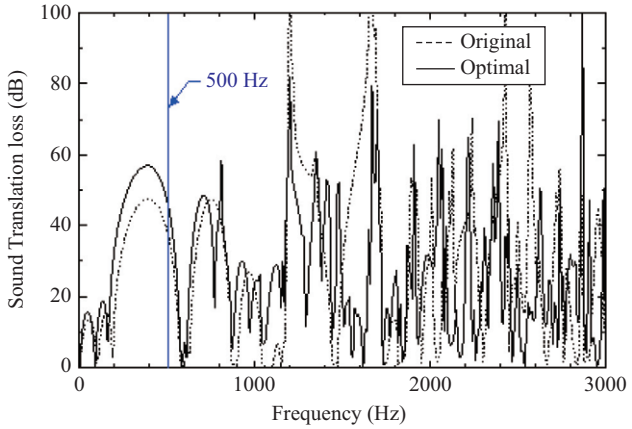

Fig. 8. Comparison of the STL of muffler B before and after optimization is performed (target tone: 500 Hz).

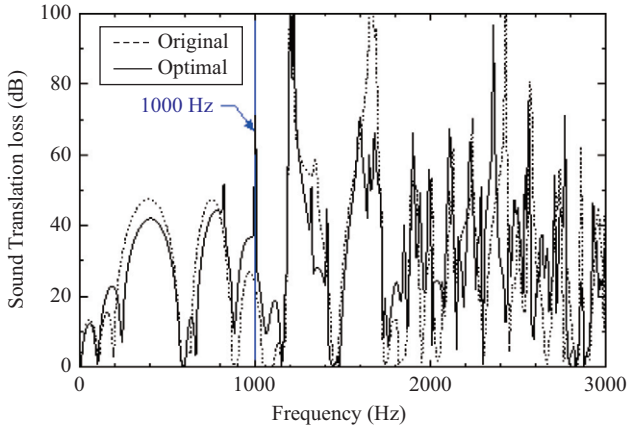

Fig. 11. Comparison of the STL of muffler B before and after optimization is performed (target tone: 1000 Hz).

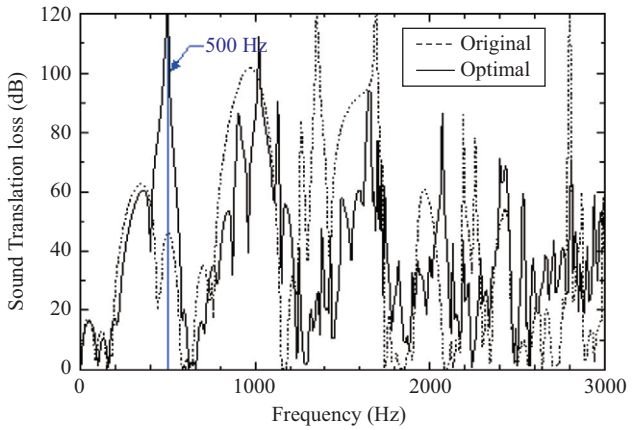

Fig. 9. Comparison of the STL of muffler C before and after optimization is performed (target tone: 500 Hz).

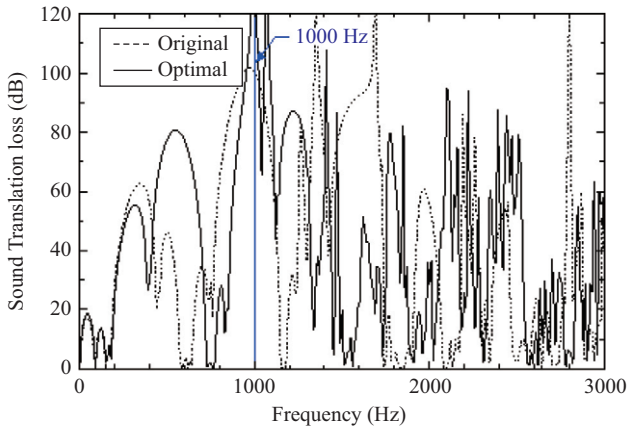

Fig. 12. Comparison of the STL of muffler C before and after optimization is performed (target tone: 1000 Hz).

STLs of the mufflers have been precisely maximized at the targeted tones. As indicated in Table 3, the STL with respect to mufflers A to C at 500 Hz has been improved by 76 dB, 11 dB, and 80 dB. Similarly, as depicted in Table 4, the STL with respect to mufflers A to C at 1000 Hz has been improved by 47 dB, 45 dB, and 94 dB. Likewise, as illustrated in Table 5, the STL

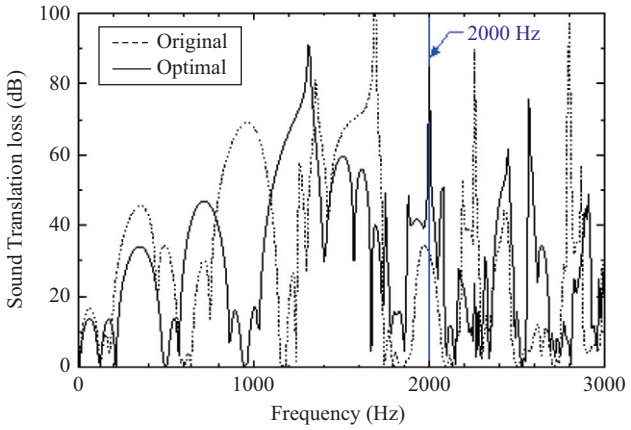

Fig. 13. Comparison of the STL of muffler A before and after optimization is performed (target tone: 2000 Hz).

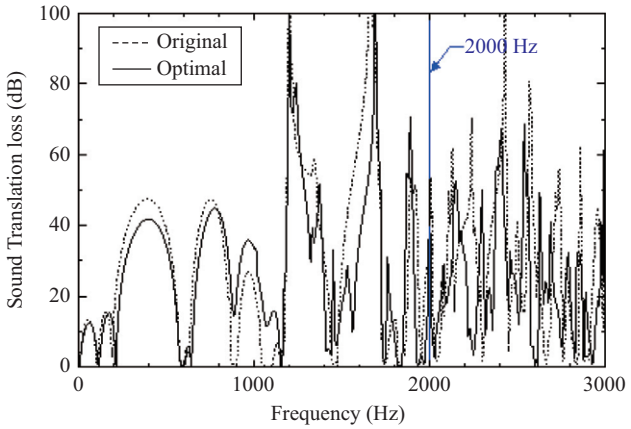

Fig. 14. Comparison of the STL of muffler B before and after optimization is performed (target tone: 2000 Hz).

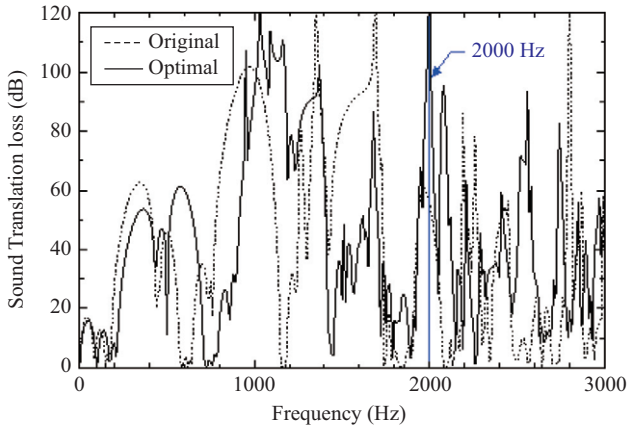

Fig. 15. Comparison of the STL of muffler C before and after optimization is performed (target tone: 2000 Hz).

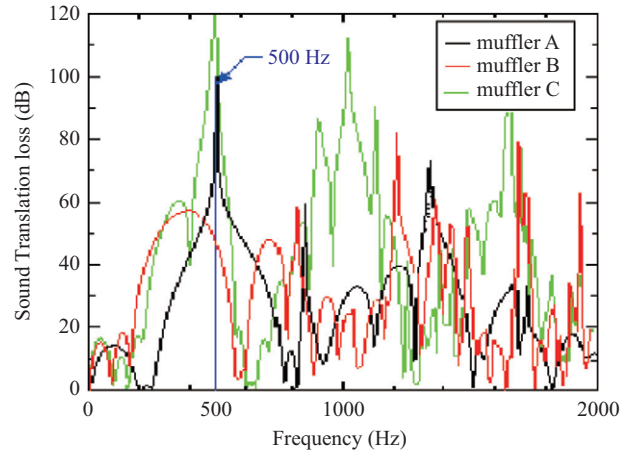

Fig. 16. Comparison of the STL of mufflers A to C after optimization is performed (target tone: 500 Hz).

with respect to mufflers A to C at 2000 Hz has been improved by 55 dB, 16 dB, and 84 dB.

As indicated in Table 3 and Fig. 16, the STL with respect to mufflers A-C at target tone (500 Hz) reaches 110 dB, 47 dB, and 125 dB. Likewise, as indicated in Table 4, the STL with respect to mufflers A-C at target tone (1000 Hz) reaches 115 dB, 70 dB, and 194 dB. Also, as illustrated in Table 5, the STL with respect to mufflers A-C at target tone (2000 Hz) is 85 dB, 43 dB, and 140 dB. Obviously, muffler C (a four-chamber muffler composed of two reverse chambers and two straight chambers) has the best acoustical performance. Moreover, the STL of muffler A (a three-chamber muffler composed of two straight chambers and a reverse chamber) is better than that of muffler B (a three-chamber muffler composed of three reverse chambers). Here, considering the geometric limit (structure beam) inside the building, the number of muffler A's geometrical design parameter available to use to reach optimal STL by adjusting the muffler shape is four. However, the number of muffler B's available geometrical design parameters is three only. With this, the acoustical performance of B is worse than that of muffler A. In addition, more chambers in the muffler (such as muffler C) will result in a better acoustical performance.

VII. CONCLUSION

It has been shown that the optimization of muffler shapes can be easily and efficiently carried out by using a four-pole transfer matrix as well as a *GA* optimizer. Considering the noise elimination of a pure tone noise propagating along the venting duct installed inside the building, three kinds of mufflers with rectangular section are adopted and optimized using GA algorithm. Optimal results in Figs. 7-15 indicate that the predicted maximal value of the *STL* can be located at the desired frequencies (500, 1000, and 2000 Hz). Hence, the tuning ability established by adjusting the design parameters of mufflers A-C in conjunction with GA method is assured. Moreover, as indicated in Figs. 7-16, the STL profile of muffler C (a four-chamber muffler composed of two reverse chambers and two straight chambers) is better than that of muffler A (a three-chamber muffler composed of two straight chambers and a reverse chamber) and

muffler B (a three-chamber muffler composed of three reverse chambers).

Consequently, results reveal that more number of muffler's geometrical design parameters used in optimization process will obtain better acoustical performance. In addition, more chambers used in the muffler will result in a better acoustical performance.

VIII. NOMENCLATURE

This paper is constructed on the basis of the following notations:

c_0: sound speed (m/s)
f: frequency (Hz)
ω: angular frequency (= $2\pi f$) (rad/s)
ρ_0: air density (kg/m^3)
m, n: acoustical mode
k: wave number of sound wave $\left(\frac{\omega}{c_o}\right)$
k_x: wave number of sound wave in x-axis $\left(\frac{m\pi}{b}\right)$
k_y: wave number of sound wave in y-axis $\left(\frac{n\pi}{h}\right)$
k_z: wave number of sound wave in z-axis $\sqrt{k^2-k_x^2-k_z^2}$
b: width of expansion chamber (m)
h: height of expansion chamber (m)
l: length width of expansion chamber (m)
b_1: width of inlet (m)
h_1: height of inlet (m)
b_2: width of outlet (m)
h_2: height of outlet (m)
(b_{c1}, h_{c1}): center coordinate of inlet (m)
($_{bc2}$, h_{c2}): center coordinate of outlet (m)
S_0: section area of the expansion chamber (m^2)
S_1: section area of inlet (m^2)
S_2: section area of outlet (m^2)
U_i: acoustical volume velocity (m^3/s)
Z_0: acoustical impedance of the expansion chamber in z-axis (rayls/m)
Z_1: acoustical impedance of inlet in z-axis (rayls/m)
Z_2: acoustical impedance of outlet in z-axis (rayls/m)
$\overline{p}_{ii}$: averaged acoustical pressure (Pa)
$\overline{p}_{ii'}$: averaged interactive acoustical pressure (Pa)
$\overline{P}_1$: acoustical potential energy in the inlet (joule)
$\overline{P}_2$: acoustical potential energy in the outlet (joule)

ACKNOWLEDGEMENTS

The authors acknowledge the financial support of the National Science Council (MOST 104-2221-E-036-027, R.O.C.).

REFERENCES

Abom, M. (1990). Derivation of four-pole parameters including higher order mode effects for expansion chamber mufflers with extended inlet and outlet. Journal of Sound and Vibration 137, 403-418.

Chang, Y. C., L. J. Yeh and M. C. Chiu (2005). Shape optimization on double-chamber mufflers using genetic algorithm. Proc. ImechE Part C: Journal of Mechanical Engineering Science 10, 31-42.

Chang, Y. C., L. J. Yeh, M. C. Chiu and G. J. Lai (2005). Shape optimization on constrained single-layer sound absorber by using GA method and mathematical gradient methods. Journal of Sound and Vibration 286/4-5, 941-961.

Chang, Y. C., M. C. Chiu and W.C. Liu (2010). Optimization of one-chamber mufflers with perforated intruding tubes using a simulated annealing method. Journal of Marine Science and Technology 18(4), 597-610.

Chiu, M. C. and Y. C. Chang (2008). Numerical studies on venting system with multi-chamber perforated mufflers by GA optimization. Applied Acoustics. 69(11), 1017-1037.

Chiu, M. C. and Y. C. Chang (2011). Numerical assessment of two-chamber mufflers with perforated plug/non-plug tubes under space and back pressure constraints using simulated annealing. Journal of Marine Science and Technology 19(2), 176-188.

Chiu, M. C. and Y. C. Chang (2011). Numerical assessment of a venting system with multi-chamber perforated mufflers by GA method. Journal of Marine Science and Technology 19(5), 483-498.

Chiu, M. C. and Y. C. Chang (2013). Shape optimization of multi-chamber side inlet/outlet mufflers hybridized with multiple perforated intruding tubes using genetic algorithm. Journal of Marine Science and Technology 21(3), 238-249.

Chiu, M. C. (2010). Shape optimization of multi-chamber mufflers with plug-inlet tube on a venting process by genetic algorithms. Applied Acoustics 71, 495-505.

Chiu, M. C. (2010). Shape optimization of one-chamber mufflers with reverse-flow ducts using a genetic algorithm. Journal of Marine Science and Technology 18(1), 12-23.

Chiu, M. C. (2010). Numerical optimization of a three-chamber mufflers hybridized with a side inlet and a perforated tube by SA method. Journal of Marine Science and Technology 18(4), 484-495.

Chiu, M. C. (2013). Shape optimization of one-chamber perforated mufflers filled with wool using simulated annealing. Journal of Marine Science and Technology 21(4), 380-390.

Chiu, M. C. and Y. C. Chang (2014). An assessment of high-order-mode analysis and shape optimization of expansion chamber mufflers. Archives of Acoustics 39(4), 489-499.

Holland, J. (1975). Adaptation in Natural and Artificial System. Ann Arbor, University of Michigan Press, Michigan.

Ih, J. G. and B. H. Lee (1985). Analysis of higher-order mode effects in the circular expansion chamber with mean flow. Journal of the Acoustical Society of America 77, 1377-1388.

Ih, J. G. (1992). The reactive attenuation of rectangular plenum chambers. Journal of Sound and Vibration 157, 93-122.

Ih, J. G. and B. H. Lee (1987). Theoretical prediction of the transmission loss of circular reversing chamber mufflers. Journal of Sound and Vibration 112, 261-272.

Jayaraman, K. and K. Yam (1981). Decoupling approach to modeling perforated tube muffler components. Journal of the Acoustical Society of America 69(2), 390-396.

Jong, D. (1975). An Analysis of the Behavior of a Class of Genetic Adaptive Systems. Doctoral Dissertation, Department of Computer and Communication Sciences, Ann Arbor, University of Michigan, Michigan.

Mimani, A. and M. L. Munjal (2016a). Design of reactive rectangular expansion chambers for broadband acoustic attenuation performance based on optimal port location. Acoustics Austria 44(2), 299-323.

Mimani, A. and M. L. Munjal (2016b). Acoustic end-correction in a flow-reversal end-chamber muffler: A semianalytical approach. Journal of Computational Acoustics 24, 1650004.

Munjal, M. L. (1975). Velocity ratio-cum-transfer matrix method for the evalua-

tion of a muffler with mean flow. Journal of Sound and Vibration 39(1), 105-119.

Munjal, M. L. (1987). A simple numerical method for three-dimensional analysis of simple expansion chamber mufflers of rectangular as well as circular cross-section with a stationary medium. Journal of Sound and Vibration 116, 71-88.

Selamet, A. and Z. L. Ji (1998). Acoustic attenuation performance of circular flow-reversing chambers. J. Acoust. Soc. Am. 104, 2867-2877.

Seybert, A. F. and C. Y. R. Cheng (1987). Application of the boundary element method to acoustic cavity response and muffler analysis. Transactions of the American Society of Mechanical Engineers, Journal of Vibration, Stress, and Reliability in Design 109, 15-21.

Sullivan, J. W. and M. J. Crocker (1978). Analysis of concentric-tube resonators having unpartitioned of cavities. Journal of the Acoustical Society of America 64(1), 207-215.

Sullivan, J. W. (1979). A method for modeling perforated tube muffler components. I. theory. Journal of the Acoustical Society of America 66(3), 772-778.

Venkatesham, B., M. Tiwari and M. L. Munjal (2009). Transmission loss analysis of rectangular expansion chamber with arbitrary location of inlet/outlet by means of Green's functions. Journal of Sound and Vibration 323 (3), 1032-1044.

Yeh, L. J., Y. C. Chang, M. C. Chiu and G. J. Lai (2004). GA optimization on multi-segments muffler under space constraints. Applied Acoustics 65(5), 521-543.

Yeh, L. J., Y. C. Chang and M. C. Chiu (2006). Numerical studies on constrained venting system with reactive mufflers by GA optimization. International Journal for Numerical Methods in Engineering 65, 1165-1185.

Young, C. I. and M. J. Crocker (1975). Prediction of transmission loss in mufflers by the finite-element method. Journal of the Acoustical Society of America 57, 144-148.